International Journal of Applied Mechanics
Vol. 13, No. 2 (2021) 2150016 (24 pages)

DOI: 10.1142/S1758825121500162

World Scientific
www.worldscientific.com

Reduced-Order Model Description of Origami Stent Built with Waterbomb Pattern

Guilherme V. Rodrigues* and Marcelo A. Savi†

Universidade Federal do Rio de Janeiro
COPPE – Department of Mechanical Engineering
Center for Nonlinear Mechanics
21.941.972 – Rio de Janeiro – RJ, Brazil
**guilherme_@live.co.uk*
†*savi@mecanica.coppe.ufrj.br*

Received 11 September 2020
Revised 8 February 2021
Accepted 8 February 2021
Published 31 March 2021

Origami-inspired structures have found many innovative applications in engineering fields. The expressive volume changes intrinsically related to their geometry is very useful for different purposes. Nevertheless, the mathematical description of origami structures is complex, which makes the design a challenging topic. This work deals with the use of reduce-order models for the origami description. A cylindrical origami structure with waterbomb pattern, called origami stent, is of concern. A reduced-order model (ROM) is developed based on kinematics and symmetry hypotheses. Afterward, a finite element analysis (FEA) is developed based on a nonlinear bar-and-hinge model. Numerical simulations are carried out evaluating the ROM validity range. Rigid and non-rigid situations are investigated showing that ROM is able to be employed for origami description.

Keywords: Origami; kinematics; reduced-order model; finite element analysis.

1. Introduction

Origami is the art of paper folding with vast aesthetic concept that recently has found many applications in engineering fields, giving rise to the origami-inspired structures. The essential characteristic of origami is the creation of a three-dimensional structure from a bi-dimensional one through folding sequences. Therefore, it draws attention in situations where deployment and save space are necessary [Turner *et al.*, 2016]. In general, origami geometries are complex which makes the folding and motion analyses to be complex and related to a lot of effort [Debnath and Fei, 2013].

Advantages of origami-inspired structures include intrinsic synchronized movements, expressive volume changes and lightweight [Schenk *et al.*, 2013; Morgan *et al.*,

†Corresponding author.

2016; Jasim and Taheri, 2018]. Such advantages are of special interest in aerospace and biomedical applications [Johnson *et al.*, 2017], but robotics is another field with several applications due to ability to undergo large displacements [Fonseca and Savi, 2020; Edmondson *et al.*, 2013; Vander Hoff *et al.*, 2014]. These structures have also been employed as an energy absorption device since the origami technique enables a thin-walled tube to follow a pre-determined failure mode and to improve its energy absorption efficiency [Zhou *et al.*, 2017].

All these applications are strictly connected to innovative ideas of active materials that are able to promote a multiphysics conversion, converting a form of energy into mechanical work, performing the folding behavior of interest. The main goal is to expand structures with the application of an external field instead of external loads [Onal *et al.*, 2012; Salerno *et al.*, 2016; Lee *et al.*, 2017; Chen *et al.*, 2019]. In this regard, the use of active materials in origami-inspired structures is wide, establishing new ideas of self-expandable structures [Peraza-Hernandez *et al.*, 2014]. In particular, it is noted that the use of shape memory alloys as actuators in the origami creases seems to be promising since they can promote the origami deployment in an effective way [Ansari *et al.*, 2018].

Origami modeling is usually established by two approaches: one treats the kinematics of the structure, considering a rigid origami where the creases are modeled as hinges and the panels between the creases are rigid, without stretch or bend; the second approach considers the flexibility of thin sheets, where panel deformation adds degrees of freedom (DoF) to the model. Usually, this approach is built using finite element models and provides thorough information about strain and stress distributions. Although this analysis provides a good description, it is computationally expensive and requires a detailed information of the design [Liu and Paulino, 2016]. On the other hand, kinematics modeling is essential to the analysis and design of origami structures [Peraza-Hernandez *et al.*, 2016]. It is usual to consider a zero-thickness sheet hypothesis to build the model [Lang *et al.*, 2018].

Even though non-rigid origami is a more realistic model, rigid origami formulation is sufficient in plenty of cases [Tachi, 2010]. Symmetry assumptions allow the construction of reduced-order models (ROMs) that are interesting to describe the origami behavior, especially in dynamical analysis [Fonseca and Savi, 2020; Fonseca *et al.*, 2019; Rodrigues *et al.*, 2017].

A tubular origami structure named origami stent is the focus of this work. Stent is a medical device used to open up a blocked lumen and protect a weakened lumen in the human body. Usually, stents are made of a wire frame while stent grafts use a thin cover attached to the stent. The term origami stent is employed in this work to represent the stent graft that was first explored by Kuribayashi *et al.* [2006] as a structure that can change its radius significantly. Different materials are investigated into the literature as stent graft actuator, as for example, shape memory alloys [Rodrigues *et al.*, 2017] and shape memory polymers [Liu *et al.*, 2019, 2020]. Both of them present good biocompatibility and biodegradability.

This paper deals with the description of origami stent using a ROM. A kinematics analysis is developed considering different symmetry hypotheses. Results predicted by this model is compared with a mechanical analysis based on finite element analysis (FEA). A quasi-static bar-and-hinge model with an implicit nonlinear displacement-based formulation is performed based on the Liu and Paulino [2017] analysis using the MERLIN code. Results define the validity range of the main hypotheses, showing that the ROM description is useful for several purposes.

After this introduction, this paper is organized as follow. An overview of the origami stent characteristics is presented in Sec. 2. In Sec. 3, the ROM based on kinematics analysis with different symmetry hypotheses is presented. Section 4 describes the mechanical analysis based on FEA. A comparison between models is presented in Sect. 5. Finally, Sec. 6 presents the conclusions of this work.

2. Origami Stent

Origami stent is a cylindrical structure built with waterbomb pattern and first presented by Kuribayashi *et al.* [2006] as a new foldable stent graft (Fig. 1). It is an expandable structure that can change considerably its radius promoting the stiffness increase, and being able to be applied in lumen, general pipes and oil drilling wells.

Origami stent is built from a tessellation of a folding pattern repetitively ordered in a sequence presented in Fig. 2. This waterbomb based pattern consists of six creases, two mountains and four valley creases, around a central vertex, being investigated in some references [Hanna *et al.*, 2014; Chen *et al.*, 2016]. The more usual configuration of the waterbomb pattern is a square shape with $L = L_2$, which means $\alpha_0 = 45^\circ$ ($L_2 = L \tan \alpha_0$).

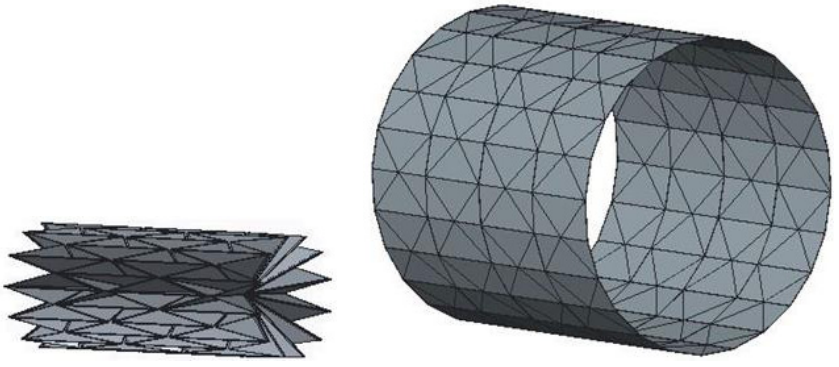

(a) (b)

Fig. 1. Origami stent, a cylindrical origami structure with expandable characteristics. Stage (a) and (b) present a closed and an open configuration, respectively after folding deployment where a significantly radius change is perceptible.

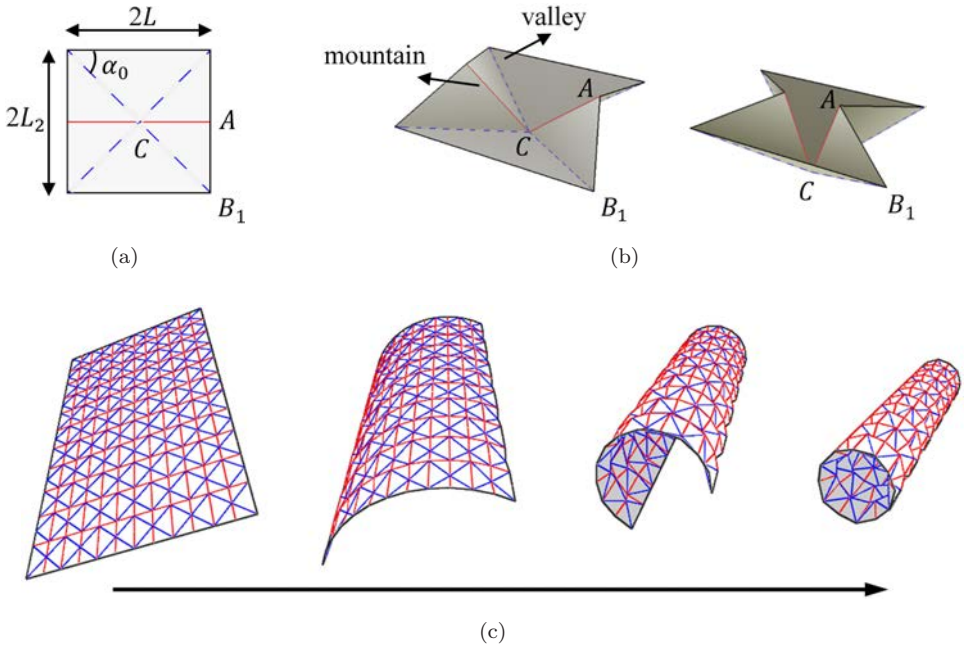

Fig. 2. (Color online) Origami stent folding pattern is given by the repetition of a unit cell (a). Red lines represent mountain folds and blue lines represent valley fold as indicate in (b). This unit cell is known as waterbomb base. In a planar sheet, these unit cells are in rows half-unit shifted of each other and sheet extremities are connected to form a cylindrical shape (c).

The analysis of the origami stent needs the evaluation of the waterbomb pattern that is a multi- DoF system. A unit cell can be described by a spherical $6R$ linkage with three DoF [Chen *et al.*, 2016] and the connection of several unit cells increases significantly the DoF of the structure. In this regard, symmetry hypotheses are interesting in order to define a proper number of the necessary DoF for the origami description.

3. Reduced-Order Model

In this section, a ROM is formulated for the origami stent based on symmetry hypotheses. It is assumed that there is no stretching in the structure, which means that the panels remain straight during all the folding process and the folding occurs only in the creases.

Figure 3 presents an origami unit cell showing that for each crease, there is an associated angle between the adjacent panels (α_1–α_6). These angles are geometrically coupled and Fig. 4 illustrates some aspects related to the symmetry possibilities. For the sake of simplicity, it is assumed a plane-symmetry state, where there are two pairs of equal angles ($\alpha_2 = \alpha_6$ and $\alpha_3 = \alpha_5$). This hypothesis reduces the number of DoF, being plausible in real structures when subjected to certain

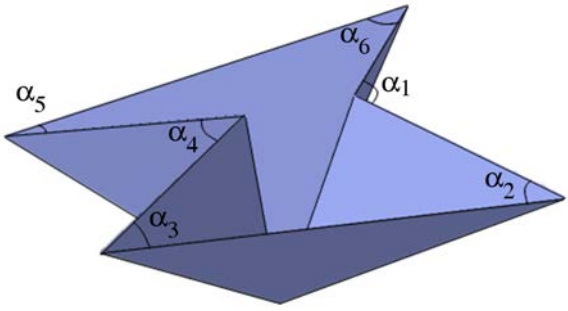

Fig. 3. Waterbomb base geometry can be described with even six angles (α_1–α_6) defined in the crease between panels. Symmetric waterbomb base can be achieved if some angles are equal to each other.

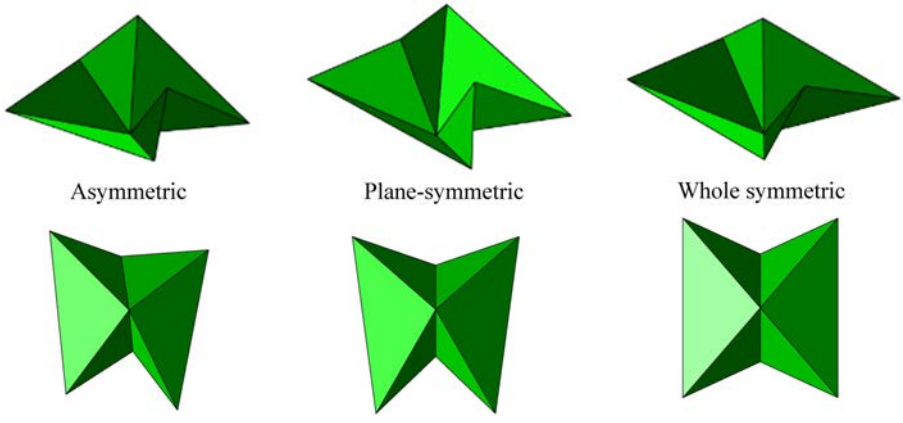

Fig. 4. Symmetry considerations about origami unit cell: asymmetric, plane-symmetric and whole symmetric waterbomb base. Bottom side of figure shows top view where presence of symmetry is more evident. In a plane-symmetric base $\alpha_2 = \alpha_6$ and $\alpha_3 = \alpha_5$ and in a whole symmetric base $\alpha_2 = \alpha_3 = \alpha_5 = \alpha_6$.

types of load [Liu *et al.*, 2014; Feng *et al.*, 2018]. If these four angles are equal ($\alpha_2 = \alpha_3 = \alpha_5 = \alpha_6$) and consequently $\alpha_1 = \alpha_4$, it is a whole symmetric case and there is a single degree of freedom [Rodrigues *et al.*, 2017].

Under plane-symmetry assumption, four angles are defined for the waterbomb base description: φ_R, φ_L, θ_R and θ_L (Fig. 5). A local coordinate frame is defined with the origin at the central vertex and the other six vertex coordinates are described as a function of these four angles.

The coordinates of the vertex are presented in the sequence. Coordinates of B_2 are equal to coordinates of B_1 but with a negative value in y and similar to B_2'. The angle α_0 (Fig. 2(a)) is commonly 45° since a square waterbomb base is considered.

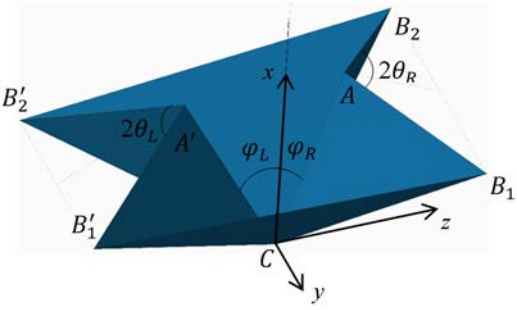

Fig. 5. A plane-symmetric waterbomb base. A local coordinate frame with origin in the central vertex is considered and four angles, φ_R, φ_L, θ_R and θ_L, are presented for its geometric description. Index $_R$ and $_L$ represent right and left side of the base, respectively. The right side is assumed in the positive z direction.

In the following sections, this angle is omitted due to that.

$$A = L\begin{bmatrix}\cos(\varphi_R)\\ 0\\ \sin(\varphi_R)\end{bmatrix} \tag{1}$$

$$A' = L\begin{bmatrix}\cos(\varphi_L)\\ 0\\ -\sin(\varphi_L)\end{bmatrix} \tag{2}$$

$$B_1 = L\begin{bmatrix}\cos(\varphi_R) - \tan(\alpha_0)\sin(\varphi_R)\cos(\theta_R)\\ \tan(\alpha_0)\sin(\theta_R)\\ \sin(\varphi_R) + \tan(\alpha_0)\cos(\varphi_R)\cos(\theta_R)\end{bmatrix} \tag{3}$$

$$B_1' = L\begin{bmatrix}\cos(\varphi_L) - \tan(\alpha_0)\sin(\varphi_L)\cos(\theta_L)\\ \tan(\alpha_0)\sin(\theta_L)\\ -\sin(\varphi_L) - \tan(\alpha_0)\cos(\varphi_L)\cos(\theta_L)\end{bmatrix} \tag{4}$$

By assuming a rigid origami, the distance between adjacent vertices is constant. Thus, the distance $\overline{B_1B_1'}$ measures $2L$. Considering Eqs. (3) and (4), the following relationship among the four angles can be found:

$$\begin{aligned}&\tan^2(\alpha_0)[\cos\theta_L\cos\theta_R(\cos(\varphi_L+\varphi_R)) - \sin\theta_L\sin\theta_R + 1]\\ &\quad + \tan(\alpha_0)[\sin(\varphi_L+\varphi_R)(\cos\theta_L + \cos\theta_R)] - \cos(\varphi_L+\varphi_R) = 1\end{aligned} \tag{5}$$

This equation gives a relation for any plane-symmetric rigid waterbomb pattern unit cell. The next modeling step is to analyze the tessellation, the combination of unit cells. Consider a row of n unit cells, circumferentially connected (Fig. 6) to

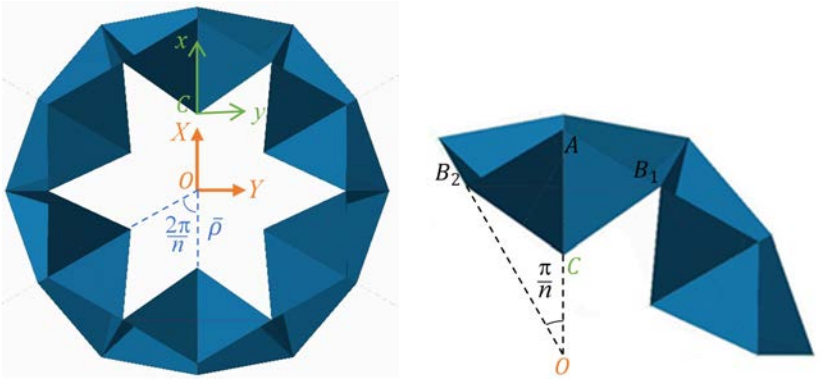

(a) (b)

Fig. 6. A row of an origami stent composed of six unit cells ($n = 6$). Each unit cell has a local coordinate frame xyz. The global coordinate frame is XYZ with origin in the center of the cylindrical structure. Since all unit cells have the same behavior, $\bar{\rho}$ (distance $\bar{\text{OC}}$) represents an internal radius of the cylindrical structure.

form a cylindrical structure. A hypothesis of circumferential symmetry is adopted, which means that each unit cell has the same behavior during all the structure deployment. Therefore, it is possible to define a global coordinate frame for the cylindrical structure.

The distance between the local coordinate xyz and the global coordinate frame XYZ (distance $\bar{\text{OC}}$) is defined as $\overline{\rho}$ and it can be considered as an internal radius of the cylindrical structure; when $\bar{\rho}$ vanishes, it indicates a completely closed configuration. With the aid of Fig. 6 and Eqs. (3) and (4), it is possible to find the following relations:

$$\rho = \frac{\bar{\rho}}{L} = \frac{1}{\tan\left(\frac{\pi}{n}\right)} \tan(\alpha_0)\sin(\theta_R) - \cos(\varphi_R) + \tan(\alpha_0)\sin(\varphi_R)\cos(\theta_R) \tag{6}$$

$$\rho = \frac{\bar{\rho}}{L} = \frac{1}{\tan\left(\frac{\pi}{n}\right)} \tan(\alpha_0)\sin(\theta_L) - \cos(\varphi_L) + \tan(\alpha_0)\sin(\varphi_L)\cos(\theta_L) \tag{7}$$

A new equation may be written making Eq. (6) to (7), furnishing a relationship among the four angles, as in Eq. (5), but considering circumferential symmetry together with unit cell plane-symmetry. Based on that, for a row of waterbomb unit cells in a cylinder, once two angles are known, the other two angles can be found by solving the system of Eqs. (5)–(7). Since the solution of this system is too long, it is not explicitly presented here. Nevertheless, it is important to highlight that once known φ_L and θ_L system's solution furnishes φ_R and θ_R or the inverse.

Origami stent is made of several rows shifted (Fig. 2(a)). It should be noted that there are vertices in a row that connect to the adjacent row. By considering the index j to indicate the row, Fig. 7 shows that vertex $A_{j=1}$ is equivalent to $B'_{2_{j=2}}$ and $B_{1_{j=1}}$ is equivalent to $A'_{j=2}$. With the help of Eqs. (1)–(4), (6) and (7), it is

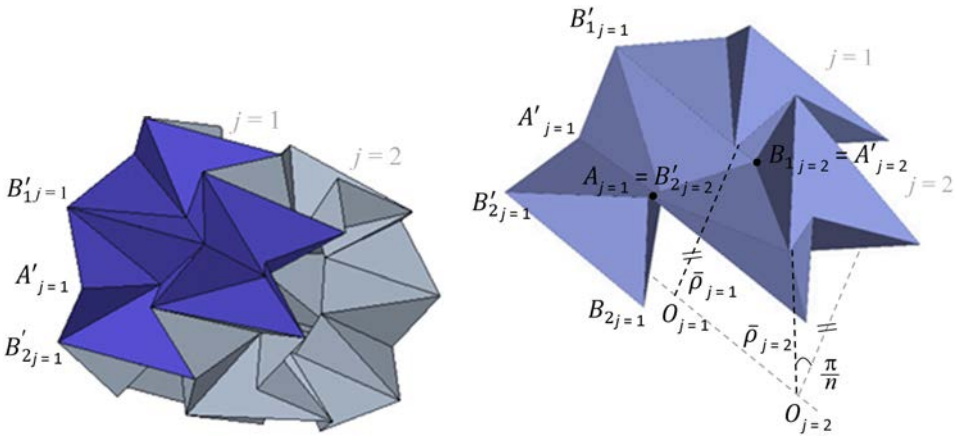

(a) (b)

Fig. 7. Highlight of three unit cells of the origami stent. Coincident vertices (for example, $A_{j=1}$ and $B'_{2_{j=2}}$) help to understand geometric relations between unit cells of different rows.

possible to find the following two relations:

$$\theta_{L_{j+1}} = \sin^{-1}\left(\frac{1}{\tan(\alpha_0)}\left(\rho_j + \cos(\varphi_{R_j})\sin\left(\frac{\pi}{n}\right)\right)\right) \tag{8}$$

$$\varphi_{L_{j+1}} = \sin^{-1}\left(\frac{\sin(\theta_{L_j}) - \sin(\theta_{L_{j+1}})\cos\left(\frac{\pi}{n}\right)}{\cos(\theta_{L_{j+1}})\sin\left(\frac{\pi}{n}\right)}\right) \tag{9}$$

Under these assumptions, it should be pointed out that knowing two angles of a row allows one to find the other two by solving a system of equations and this row is well defined. Therefore, two angles of adjacent rows are found using Eqs. (8) and (9). Once again, the other two angles can be found by solving the system of equations. Thereby, knowing only two angles, it is possible to characterize the whole geometry of the origami stent with different number of rows, considering circumferential symmetry (all unit cells in a row present the same behavior) and unit cell plane-symmetry.

Origami stent geometry is entirely defined by these simple equations under symmetry hypothesis. It is emphasized that it is necessary that the knowledge of two angles in a row solve the system of equations that furnishes the other two angles of the same row and once a row is well defined, the adjacent rows can also be geometrically defined by Eqs. (8) and (9). Therefore, if a relation between these two initial angles is found, it is necessary to know only one of them to describe the whole structure. This can be achieved going further on symmetry hypotheses. By assuming a bilateral symmetry, the origami stent has two equal halves (Fig. 8). In this case, there are two possible formulations: for an odd number of rows and for an even number of rows.

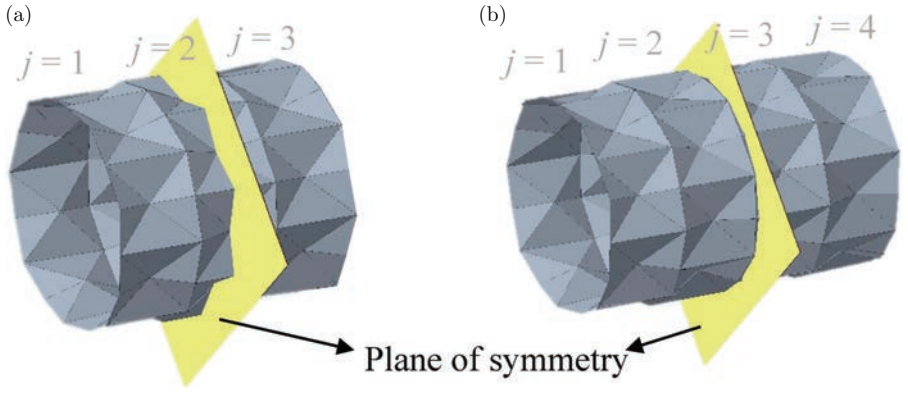

Fig. 8. Origami stent with two equal halves divided by a plane of symmetry. It is called origami stent with bilateral symmetry. For an odd number of rows (a), the middle row is halved then the unit cells of this row must be whole symmetric. It does not happen for an even number of rows (b).

Let m be the number of rows in the origami stent. By considering m an odd number, it is necessary that the waterbomb unit cell in the middle of the structure is wholly symmetric (see row $j = 2$ on Fig. 8(a)), that is, $\varphi_{R_2} = \varphi_{L_2}$ and $\theta_{R_2} = \theta_{L_2}$. Therefore, only two angles describe the unit cell of the middle row but it is necessary to know only one to find another one by using Eq. (5). Once the middle row is defined, the angles of adjacent rows can be found as previously described considering unit cells plane-symmetric.

For instance, the general case where all unit cells are plane-symmetric needs two angles of any row to be entirely defined, which means that it is a 2-DoF system. If the structure has a bilateral symmetry as in Fig. 8(a), it can be reduced to 1-DoF system and it is necessary to know just one angle of the middle row.

By considering an origami with an even number of rows (m is even), a row in the left side of the plane-symmetry must have a mirrored behavior of a row in the right side. For example, in Fig. 8(b), $\varphi_{R_2} = \varphi_{L_3}$, $\theta_{R_2} = \theta_{L_3}$ and vice-versa. Using coordinates of vertices A', B_1' and B_2' defined by Eqs. (1)–(4) (Fig. 7) of the row $j = 3$, it is possible to find a relation for θ_{L_3} as a function of φ_{R_2} and θ_{R_2}. As in this case $\theta_{L_3} = \theta_{R_2}$, with the aid of Eqs. (6) and (7), an expression of φ_{R_2} as a function of θ_{R_2} is found, see Eq. (10). Note that this expression is only valid for the two rows in the middle (in this example, row $j = 2$ or row $j = 3$ remembering that $\varphi_{R_2} = \varphi_{L_3}$ and $\theta_{R_2} = \theta_{L_3}$).

$$\varphi_{R_2} = \tan^{-1}\left(\frac{\sin\theta_{R_2}\left(\cos\frac{\pi}{n} - 1\right)}{\sqrt{2(\sin\theta_{R_2})^2\left(\cos\frac{\pi}{n} - 1\right) + \left(\sin\frac{\pi}{n}\right)^2}}\right) \tag{10}$$

As previously described, the other angles of the origami stent structure can be defined if two angles are known. Once again, the system can be assumed as a 1-DoF system instead of 2-DoF due to the possible relation of Eq. (10).

Table 1. Physical limitations of the origami configurations. Approximate values of the minimum and maximum angle for the origami stent under symmetric hypotheses (n is the number of unit cells in a row and m is the number of rows).

	$n = 6$	$n = 8$	$n = 10$
$m = 1$	$8.3^\circ \leq \varphi_{R_1} \leq 90^\circ$	$4.6^\circ \leq \varphi_{R_1} \leq 90^\circ$	$2.9^\circ \leq \varphi_{R_1} \leq 90^\circ$
$m = 2$	$8.8^\circ \leq \varphi_{R_2} \leq 64.8^\circ$	$4.8^\circ \leq \varphi_{R_2} \leq 70.8^\circ$	$3.0^\circ \leq \varphi_{R_2} \leq 75.3^\circ$
$m = 3$	$8.3^\circ \leq \varphi_{R_2} \leq 59.3^\circ$	$4.6^\circ \leq \varphi_{R_2} \leq 67.8^\circ$	$2.9^\circ \leq \varphi_{R_2} \leq 72.6^\circ$
$m = 4$	$8.8^\circ \leq \varphi_{R_2} \leq 57.1^\circ$	$4.8^\circ \leq \varphi_{R_2} \leq 65.9^\circ$	$3.0^\circ \leq \varphi_{R_2} \leq 71.2^\circ$
$m = 5$	$8.3^\circ \leq \varphi_{R_3} \leq 56.4^\circ$	$4.6^\circ \leq \varphi_{R_3} \leq 66.3^\circ$	$2.9^\circ \leq \varphi_{R_3} \leq 71.5^\circ$

Under these assumptions, bilateral symmetry allows the description of origami stent with either an odd number or an even number of rows by a 1-DoF model. Therefore, only one angle is needed to describe the whole rigid origami stent structure.

In brief, three considerations of symmetry have to be done to allow the description of the structure as a 1-DoF model: plane symmetry of each unit cell (Fig. 4); circumferential symmetry, all unit cells in a row have the same behavior; and bilateral symmetry, plane symmetry of the whole structure (Fig. 8). The idea of plane symmetry of the unit cells is important to analyze the origami stent. Indeed, if a whole symmetric unit cell (Fig. 4) is taken for every row, origami rigid theory does not allow the structure to have more than one row [Kuribayashi, 2004].

It is important to emphasize that there is a physical limit for the origami angles that include material penetration and the transformation of a valley into a mountain or vice-versa, which may mischaracterize the origami. For example, the radius of the origami stent cannot be less than zero, otherwise it represents a material penetration. Values indicating these limits are presented in Table 1 and, out of that range, the system of equations has not a feasible solution.

4. Finite Element Analysis

Origami description can be performed by mechanical approach using the FEA. A quasi-static finite element model proposed by Liu and Paulino [2017] is adopted in this paper. The idea is to use a bar-and-hinge model with an implicit nonlinear displacement-based formulation, considering quasi-static analysis of non-rigid origamis (with deformable panels). The MERLIN code is employed to develop numerical simulations.

In a bar-and-hinge model [Shenk and Guest, 2011], an origami sheet is represented by triangular truss framework (triangular panels may not need to be divided). Figure 9 presents a schematic illustration of the model where bars are placed in fold lines and across panels for in-plane stiffness. Rotational hinges are along these bars to model folding creases or bending of panels.

The structure is assumed to be nonlinear elastic and therefore, the total potential energy Π is due to the strain energy stored in bars (U_{bar}), the strain energy stored

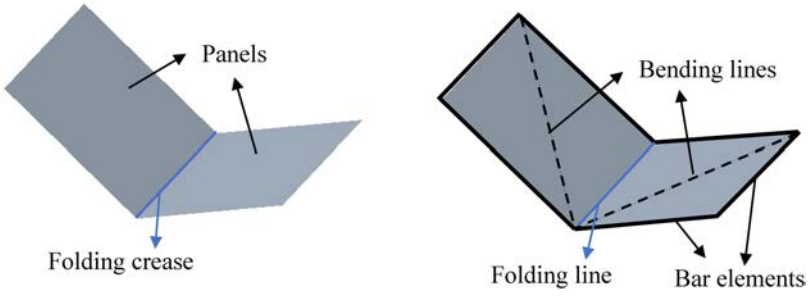

Fig. 9. Bar-and-hinge model illustration: origami panels are triangulated to a truss framework. Rotational springs are placed along folding and bending lines.

in folding deformation (U_{spr}) and the external work (V_{ext}): $\Pi = U_{\text{bar}} + U_{\text{spr}} - V_{\text{ext}}$. By assuming that $\mathbf{u}$ is the nodal displacement vector, equilibrium of the system is given by

$$\frac{\partial \Pi}{\partial \mathbf{u}} = \frac{\partial U_{\text{bar}}}{\partial \mathbf{u}} + \frac{\partial U_{\text{spr}}}{\partial \mathbf{u}} - \mathbf{F} = 0 \tag{11}$$

Derivatives of U_{bar} and U_{spr} denote internal forces and $\mathbf{F}$ denotes external forces. The tangent stiffness matrix $\mathbf{K}_T$ is a summation of the contributions from the bars and the rotational springs ($\mathbf{K}_T = \mathbf{K}_{\text{bar}} + \mathbf{K}_{\text{spr}}$). For each bar element, a stored energy density is assumed to be a function of the one-dimensional Green–Lagrange strain E_x considering both material and geometric nonlinearities. This strain also leads the evaluation of the 2nd Piola–Kirchhoff stress S_x and tangent modulus C. Thus, the tangent stiffness matrix can be expressed by

$$\mathbf{K}_{\text{bar}}^{i} = A_i L_i \left[S_x \frac{\partial^2 E_x}{\partial \mathbf{u}_i^2} + C \frac{\partial E_x}{\partial \mathbf{u}_i} \left(\frac{\partial E_x}{\partial \mathbf{u}_i} \right)^{\mathrm{T}} \right] \tag{12}$$

where A_i and L_i denotes the area and the length of the bar and $\mathbf{u}_i$ is the displacement.

Similar equation can be found for the rotational spring element as a function of the dihedral angle θ as

$$\mathbf{K}_{\text{spr}}^{q} = L_q \left[M \frac{\partial^2 \theta}{\partial \mathbf{u}_q^2} + k \frac{\partial \theta}{\partial \mathbf{u}_q} \left(\frac{\partial \theta}{\partial \mathbf{u}_q} \right)^{\mathrm{T}} \right] \tag{13}$$

where M is the resisting moment per unit length, k is the tangent rotational stiffness and $\mathbf{u}_q$ represents the displacement.

The bar elements are described by a two-term Ogden constitutive model [Ogden, 1997], being associated with a hyperplastic material represented by the following nonlinear stress–strain relationship:

$$S_x = \frac{C_0}{\beta_1 - \beta_2} [(\sqrt{2E_x + 1})^{\beta_1 - 2} - (\sqrt{2E_x + 1})^{\beta_2 - 2}] \tag{14}$$

where C_0 is the initial modulus and β_1 and β_2 are material parameters. It is adopted as $\beta_1 = 5$ and $\beta_2 = 1$ which represents a linear elastic material subjected to small strains.

In addition, torsional elements are described by a nonlinear moment-angle relationship, $M - \theta$, given by

$$M = \begin{cases} k_0(\theta_1 - \theta_0) + \frac{2k_0\theta_1}{\pi} \tan\left(\dfrac{\pi(\theta - \theta_1)}{2\theta}\right), & 0 < \theta < \theta_1 \\ k_0(\theta - \theta_0), & \theta_1 \leq \theta \leq \theta_2 \\ k_0(\theta_2 - \theta_0) + \dfrac{2k_0(2\pi - \theta_2)}{\pi} \tan\left(\dfrac{\pi(\theta - \theta_2)}{4\pi - 2\theta_2}\right), & \theta_2 < \theta < \pi \end{cases} \tag{15}$$

where θ_0 is the neutral angle where the rotational spring is at a stress-free state and θ_1 and θ_2 are parameters that define the nonlinear characteristics of the curve. Note that these parameters define the limit of a linear region and, after that, there is a stiffness hardening.

An implicit formulation is employed which means that equilibrium is reached at each converged incremental step. The nonlinear problem of Eq. (11) is solved by

(a)

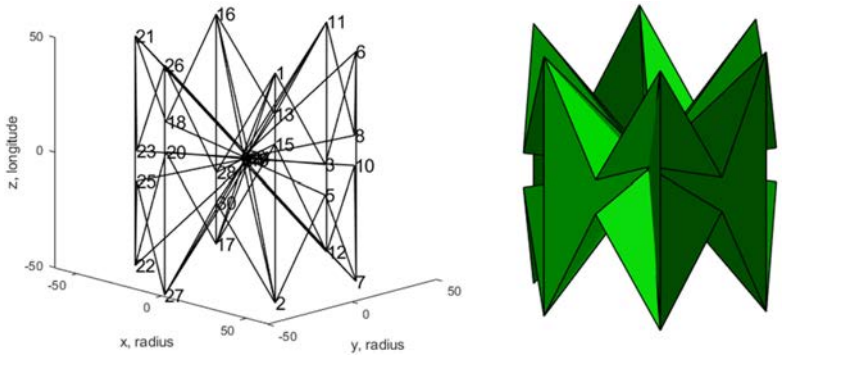

(b)

Fig. 10. Origami stent model for FEA (MERLIN code). In the waterbomb base, the load is applied in the central vertex and in the radial direction. Boundary conditions are in the lower nodes and in longitudinal direction.

an arc-length type method with an algorithm called Modified Generalized Displacement Control Method [Leon *et al.*, 2014].

Details of the formulation can be obtained on the reference paper due to Liu and Paulino [2017]. Origami stent is implemented in the MERLIN code where geometry is added as a closed configuration and loads are applied in order to promote the structure deployment. Symmetric loads are considered in order to allow a further comparison to the proposed ROM. A load is applied in the central vertex and outwards in the radial direction for every unit cell (Fig. 10), being characterized as a displacement. Boundary conditions are applied in the bottom of the origami stent (for example, in Fig. 10, nodes 2, 7, 12, 17, 22 and 27 are constrained in longitudinal direction but can move freely in radial direction). The goal is to reproduce a load type where plane-symmetry remains. Results are presented in the next section.

5. Results and Discussion

This section investigates the symmetry hypotheses by establishing a comparison between results of the ROM, developed based on kinematics analysis, and the one obtained by the mechanical analysis employing the FEA. The idea is to use conditions that establish similar behaviors of both approaches.

Results are presented as a function of $\varphi_j = \varphi_{R_j} + \varphi_{L_j}$, remembering that $j = 1, \ldots, m$ represents the number of rows and angles are represented in degree. Even though the split of this angle is used on the kinematics description, the evaluation of the entire angle is more useful since it is not bonded to a frame of reference but to the unit cell itself.

Figure 11 presents the value of the angle θ_R and of the radius ρ as a function of the angle φ considering a single row ($m = 1$) with six unit cells ($n = 6$). All the

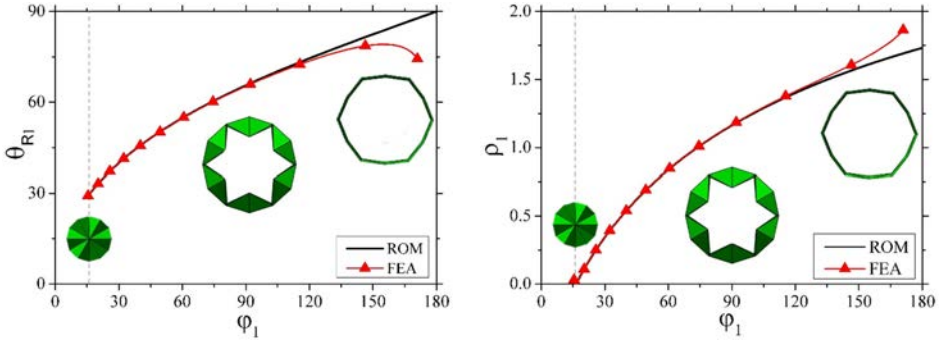

(a) (b)

Fig. 11. Comparison between ROM and FEA of an origami stent with a single row. Side view of the origami stent is presented with the graphs to aid the comprehension of the meaning of the value of φ_1. Left side (a) show the geometric relation between the angles of the unit cells and right side (b) show internal radius evolution with the angle deployment.

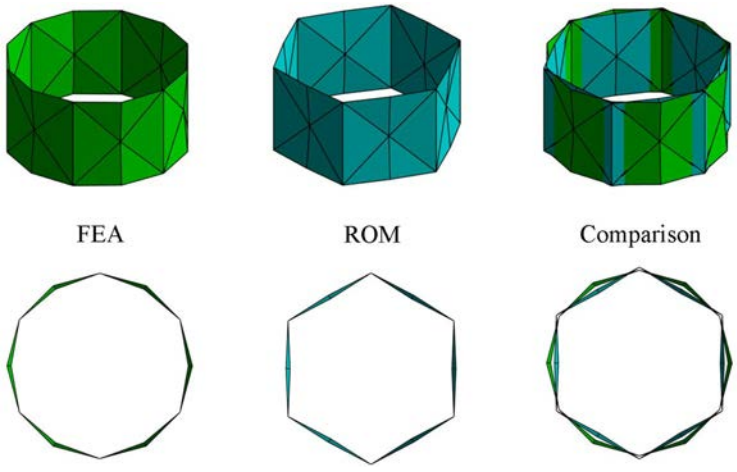

Fig. 12. Origami configurations predicted by the ROM and the FEA for $\varphi_1 = 165°$. Top side of figure presents the isometric view and bottom side of figure presents the top view of the origami stent.

unit cells have the same behavior and it is wholly symmetric, that is, $\theta_{R_1} = \theta_{L_1}$ and $\varphi_{R_1} = \varphi_{L_1}$. Dashed lines represent the limit angles based on those presented in Table 1. A side view of the origami stent represented using FEA is also presented in order to connect the angle φ_1 with the structure configuration (closed and opened). During the structure deployment, ROM and FEA present similar results until approximately $\varphi_1 = 90°$ and, after that, discrepancies occur. Figure 12 presents the difference in the final angle (approximately $\varphi_1 = 165°$) for both models.

The discrepancy between both descriptions can be explained for the stretching energy calculated by FEA. Figure 13 presents the stretching energy of a single origami row showing that whenever this energy is different from zero, the origami structure is deforming and the rigid origami hypothesis, adopted by the ROM, is not valid.

Origami panel deformation can be decreased or even avoided by considering different external loads, making results of both models closer to each other. Hence, instead of a load in the central vertex, it is assumed as a load in the longitudinal direction in the vertices A and A' (Fig. 14(d)). Under this assumption, it is noticeable that the ROM is more accurate in comparison with the FEA since the stretching energy starts to increase at a higher angle (120° instead of 90°) but also due to deformation that now occurs mostly in the longitudinal direction.

Different numbers of unit cells, n, of a single row origami stent are now of concern (Fig. 15). Results of angle and radius deployment as the stretching energy evaluated by FEA are presented in Fig. 16. It is shown that the radius depends of the parameter n but angle deployment remains unalterable which is in agreement with equations of the ROM. Besides, the stretching energy does not vary significantly (Fig. 16(c)). It should be pointed out that the maximum radius increases as a

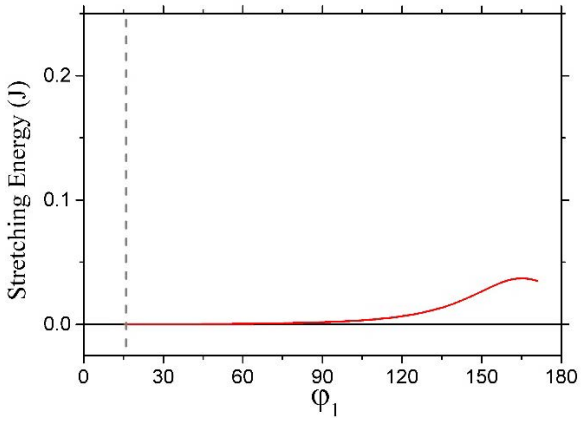

Fig. 13. Stretching energy of a single row origami stent in FEA. The increase of this energy means a stretching in the panels which goes against rigid origami theory.

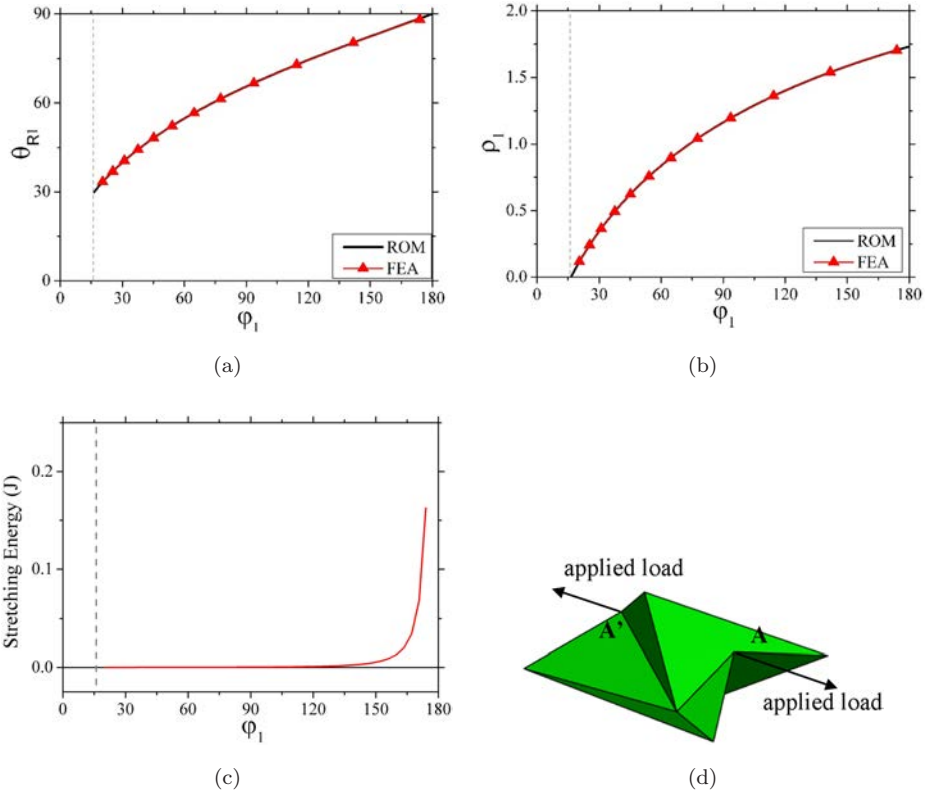

Fig. 14. Comparison of a single row origami stent deployment in the ROM and FEA considering a load applied in vertices A and A' (d). Angle deployment (a) and radius deployment (b) are equal in both models but stretching energy in FEA (c) is still valued.

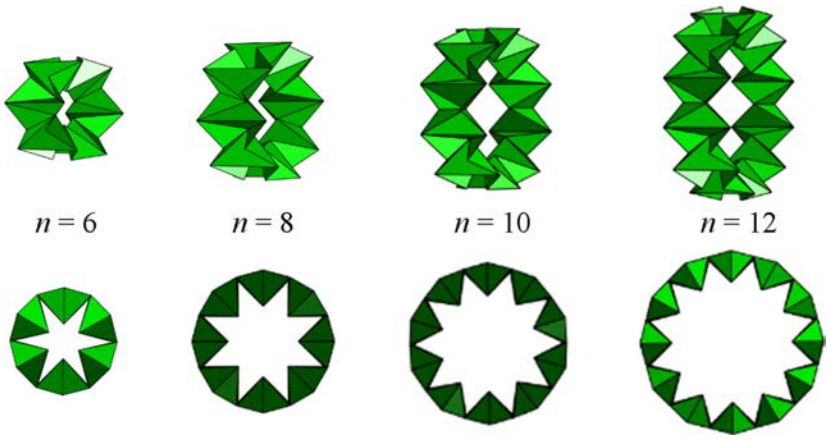

Fig. 15. A single row origami stent at $\varphi_1 = 70°$ with different n unit cells distributed circumferentially (isometric and side view). It is visible that the radius differences accordingly to the number of unit cells even though all structures have the same angle.

consequence of the increase of the number of unit cells (Fig. 16(b)). Note that, for $n = 6$, the radius almost double in a complete deployment, and it almost quadruples if $n = 12$. This aspect represents the useful origami ability of saving space.

From now on, results of six unit cells ($n = 6$) are presented. Different rows are treated, starting with a two-row origami structure ($m = 2$) (Fig. 17). In this case, waterbomb unit cells are no longer wholly symmetric but plane symmetric ($\varphi_R \neq \varphi_L$) and a row has a mirrored behavior of the other: $\theta_{R_1} = \theta_{L_2}$ and $\theta_{L_1} = \theta_{R_2}$. Figure 18 presents results as a function of φ_1 (bottom row). It is important to highlight that whilst the maximum angle for the rigid theory is reached, the structure can continue its deployment if deformation is considered.

A three-row origami ($m = 3$) is now in focus (Fig. 19). Since m is odd, middle row ($j = 2$) has a wholly symmetric behavior. Adjacent rows have the mirrored behavior among them (row 1 and row 3). Figure 20 presents the results of the origami with three rows. In comparison with the origami with one row ($m = 1$), φ_2 has a lower maximum angle since it is limited by the maximum value of φ_1. The relation between these angles is presented in Fig. 20(c).

Figure 21 presents the stretching energy estimated by the FEA for the origami stent with three rows. This energy is presented as a function of φ_1 and φ_2. Note that the peak of energy is higher than the peaks in the previous cases with one or two rows. This behavior may be associated with higher deformations and also to increase the number of unit cells in the structure since it corresponds to a total energy.

An analysis of an origami with four rows ($m = 4$) (Fig. 22) is now in focus. Figure 23 presents results of the four rows origami showing similar behavior of the previous cases. Note that the relation of the radius with the angle φ does not change for any case, which is in agreement with the ROM.

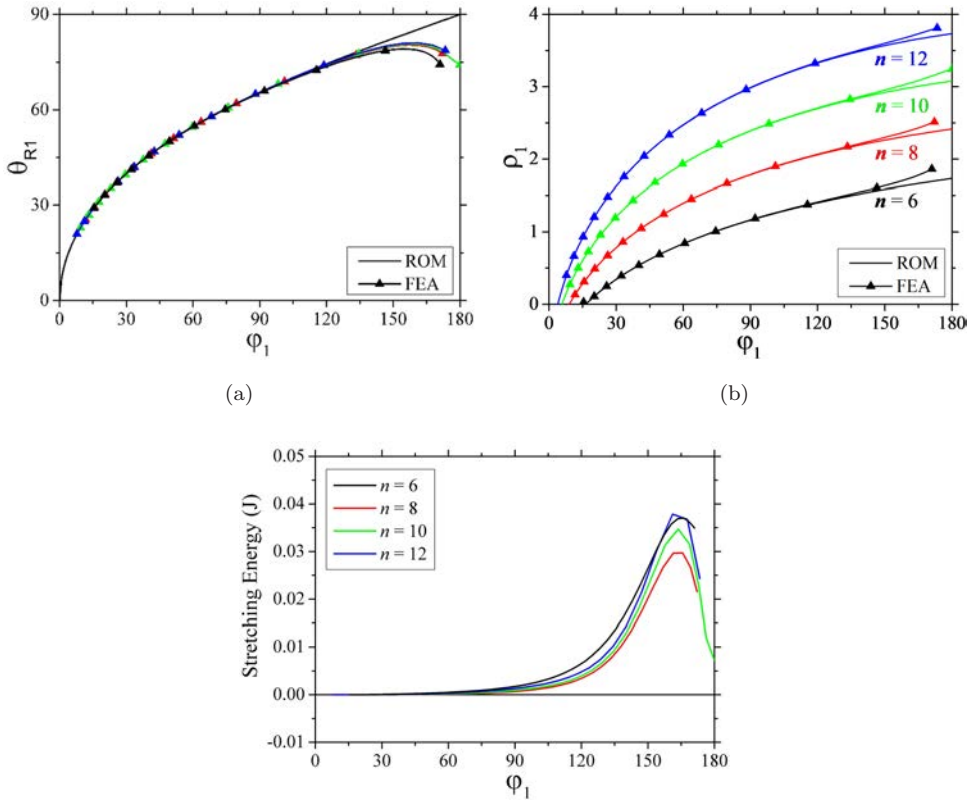

(a) (b) (c)

Fig. 16. Comparison between ROM and FEA for a single row origami stent varying the number of unit cells n. Angle deployment (a) is the same for the ROM but has some variations in the FEA. Radius deployment is presented in (b) and stretching energy in FEA in present in (c).

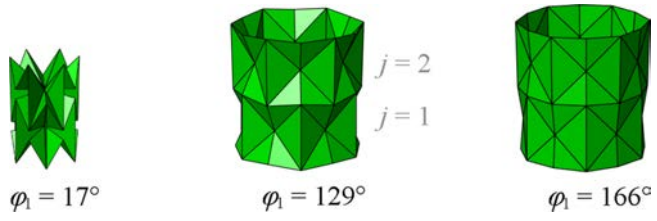

Fig. 17. Origami stent of two rows ($m = 2$) obtained by the FEA at three different stages: a closed configuration ($\varphi_1 = 17°$), a limit open configuration defined by the ROM ($\varphi_1 = 129°$) and an open configuration above that limited by the ROM ($\varphi_1 = 166°$).

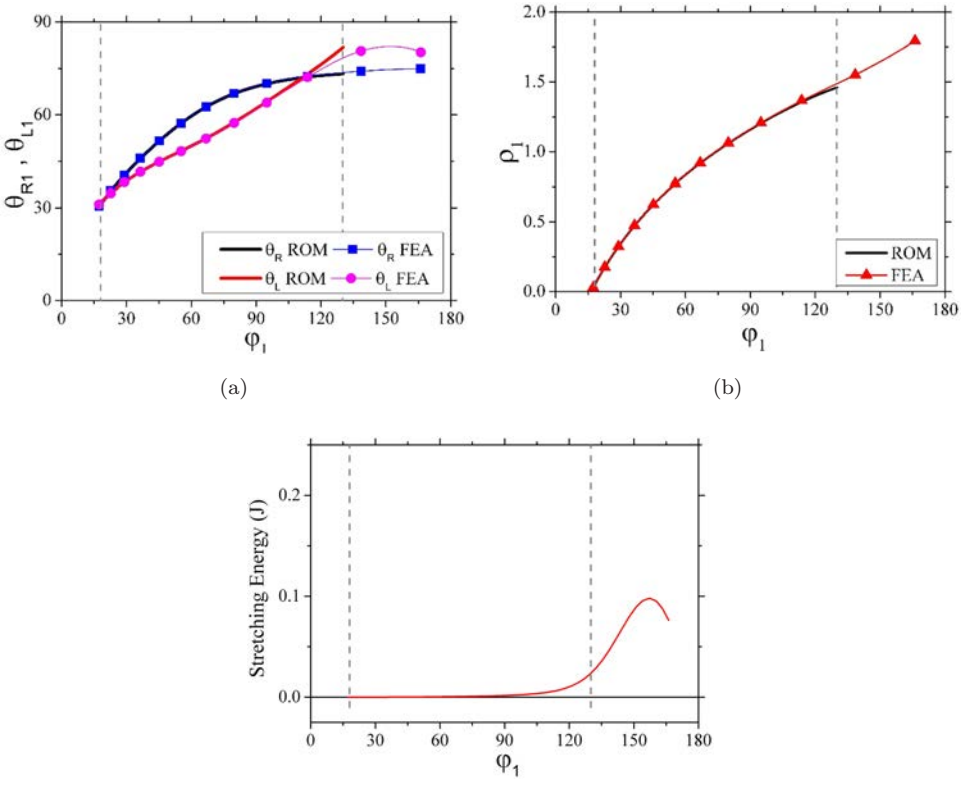

Fig. 18. Comparison between ROM and FEA for an origami stent with two rows. Angle deployment of one row is presented in (a) and radius deployment is presented in (b). Dashed lines represent limit angles of the ROM. In (c) the stretching energy is presented.

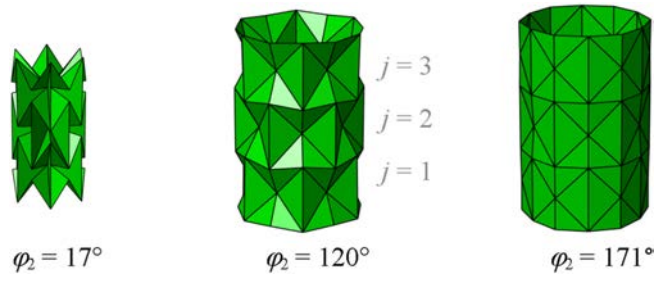

Fig. 19. Origami stent of three rows ($m = 3$) obtained by the FEA at three different stages: a closed configuration ($\varphi_2 = 17°$), a limit open configuration defined by the ROM ($\varphi_2 = 120°$) and an open configuration above that limited by the ROM ($\varphi_2 = 171°$).

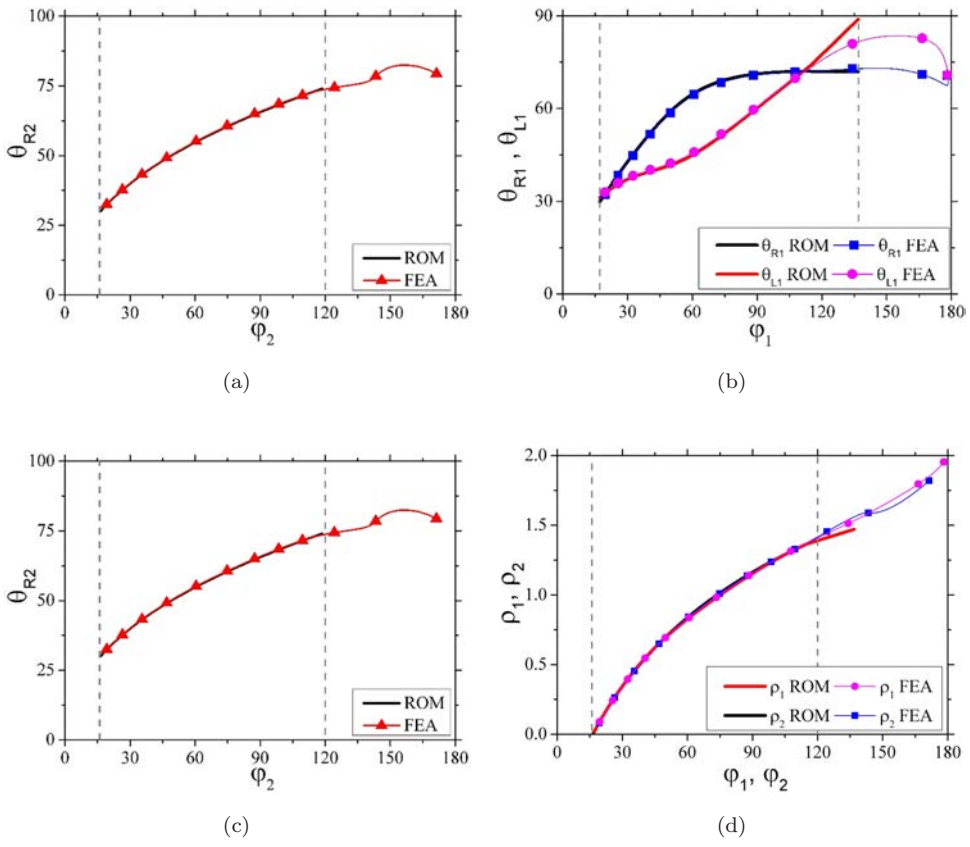

Fig. 20. Comparison between ROM and FEA for an origami stent with three rows. Angle deployment of the row $j = 2$ is presented in (a) angle deployment of the row $j = 1$ is presented in (b). The angle relation between these two rows is in (c). Radius deployment is presented in (d).

The analysis of the stretching energy is presented in Fig. 24 showing that the peak of energy is now even higher than the case of the origami with three rows, as expected. Once again, it can be justified even by higher deformations or by the increase of the number of unit cells.

In general, it is possible to say that origami description using the ROM is similar to the FEA in a certain range of validity where there is no deformation. In all cases presented, the FEA stretching energy starts to increase considerably around $\varphi_j = 105°$, which means that for angles smaller than that, there are no considerable deformations in the structure which makes both descriptions equivalent. Besides, FEA can be employed to define the limits of the origami description using ROM.

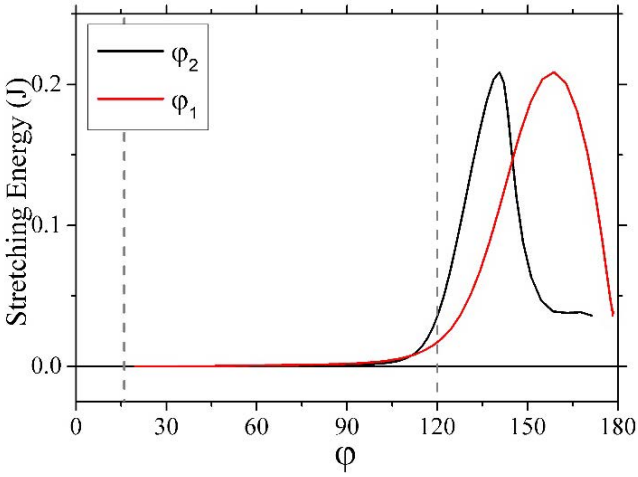

Fig. 21. Stretching energy in function of φ_1 and φ_2 for an origami stent of three rows ($m = 3$).

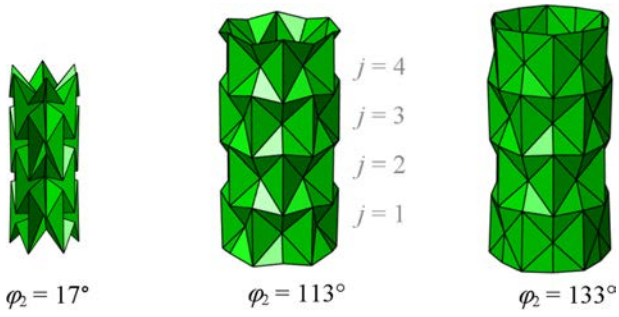

Fig. 22. Origami stent of four rows ($m = 4$) obtained by the FEA at three different stages: a closed configuration ($\varphi_2 = 17°$), a limit open configuration defined by the ROM ($\varphi_2 = 113°$) and an open configuration above that limited by the ROM ($\varphi_2 = 133°$).

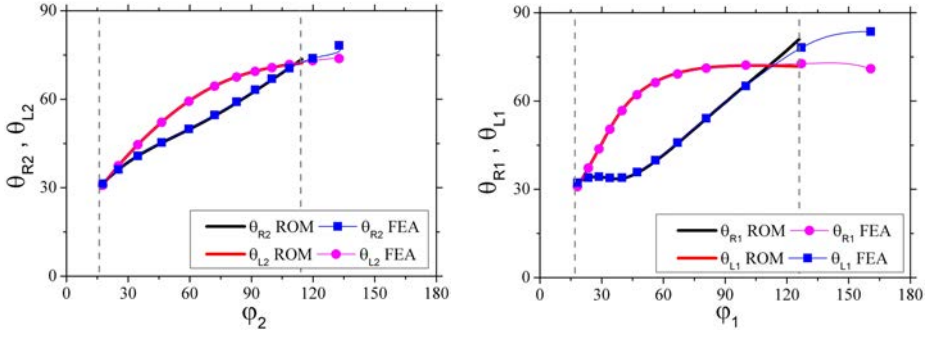

(a) (b)

Fig. 23. Comparison between ROM and FEA for an origami stent with four rows. Angle deployment of the row $j = 2$ is presented in (a) angle deployment of the row $j = 1$ is present in (b). The angle relation between these two rows is in (c). Radius deployment is presented in (d).

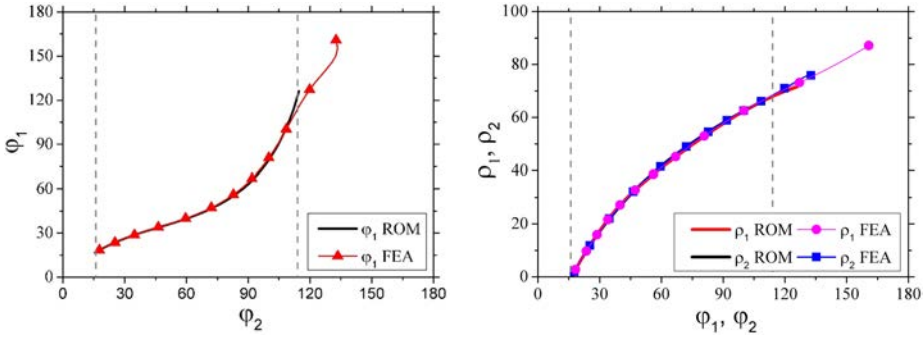

(c) (d)

Fig. 23. (*Continued*)

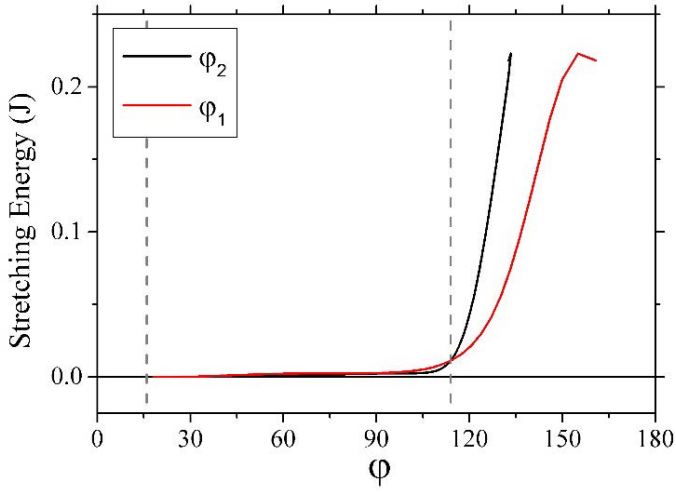

Fig. 24. Stretching energy in function of φ_1 and φ_2 for an origami stent of four rows ($m = 4$).

6. Conclusions

The analysis of an origami stent, a cylindrical origami structure, is developed considering ROM and FEA. The ROM is built based on a zero-thickness rigid origami theory and on symmetry hypotheses. Symmetry hypotheses are related to the unit cell itself and in the whole structure, considering that all unit cells have the same behavior. Different hypotheses are adopted depending on the origami configuration, defined by the number of rows. Based on that, an origami with odd number of rows requires different hypotheses than the even number. Furthermore, limit configuration should be established defining the maximum angle reached by the origami deployment. FEA is developed considering symmetric loads in order to establish a comparison with the ROM. FEA allows one to analyze non-rigid origami. In general,

both approaches are in close agreement except for conditions where panel stretch occurs. Stretch conditions start close to the upper maximum angle permitted by the ROM analysis. Based on this comparison, it is possible to establish an applicable range of angles where ROM can be employed in order to generate similar results of the FEA, being useful for different purposes. It should be pointed out that FEA can be employed to determine limit configurations, allowing an accurate origami description.

Acknowledgment

The authors would like to acknowledge the support of the Brazilian Research Agencies CNPq, CAPES and FAPERJ.

References

Ansari, M., Fahimi, P., Baghani, M. and Golzar, M. [2018] "An experimental investigation on training of NiTi-based shape memory alloys," *International Journal of Applied Mechanics* **10**(4), 1850040.

Chen, T., Bilal, O. R., Lang, R., Daraio, C. and Shea, K. [2019] "Autonomous deployment of a solar panel using elastic origami and distributed shape-memory-polymer actuators," *Physical Review Applied* **11**(6), 064069.

Chen, Y., Feng, H., Ma, J., Peng, R. and You, Z. [2016] "Symmetric waterbomb origami," *Proceedings of the Royal Society A: Mathematical, Physical and Engineering Sciences* **472**(2190), 20150846.

Debnath, S. and Fei, L. J. [2013] "Origami theory and its applications: a literature review," *World Academy of Science, Engineering and Technology* 1131–1135.

Edmondson, B. J., Bowen, L. A., Grames, C. L., Magleby, S. P., Howell, L. L. and Bateman, T. C. [2013] "Oriceps: Origami-inspired forceps," in *ASME 2013 Conference on Smart Materials, Adaptive Structures and Intelligent Systems*, American Society of Mechanical Engineers Digital Collection.

Fang, H., Li, S., Ji, H. and Wang, K. W. [2017] "Dynamics of a bistable Miura-origami structure," *Physical Review E* **95**(5), 052211.

Feng, H., Ma, J., Chen, Y. and You, Z. [2018] "Twist of tubular mechanical metamaterials based on waterbomb origami," *Scientific Reports* **8**(1), 1–13.

Fonseca, L. M. and Savi, M. A. [2020] "Nonlinear dynamics of an autonomous robot with deformable origami wheels," *International Journal of Non-linear Mechanics* **125**, 103533.

Fonseca, L. M., Rodrigues, G. V., Savi, M. A. and Paiva, A. [2016] "Nonlinear dynamics of an origami structure coupled to smart materials," in *Proceedings of the Sixth International Conference on Nonlinear Science and complexity (NSC), São Paulo, Brazil*.

Fonseca, L. M., Rodrigues, G. V., Savi, M. A. and Paiva, A. [2019] "Nonlinear dynamics of an origami wheel with shape memory alloy actuators," *Chaos, Solitons & Fractals* **122**, 245–261.

Hanna, B. H., Lund, J. M., Lang, R. J., Magleby, S. P. and Howell, L. L. [2014] "Waterbomb base: A symmetric single-vertex bistable origami mechanism," *Smart Materials and Structures* **23**(9), 094009.

Jasim, B. and Taheri, P. [2018] "An origami-based portable solar panel system," in *2018 IEEE 9th Annual Information Technology, Electronics and Mobile Communication Conference (IEMCON)* , IEEE pp. 199–203.

Johnson, M., Chen, Y., Hovet, S., Xu, S., Wood, B., Ren, H., Tokuda, J. and Tse, Z. T. H. [2017] "Fabricating biomedical origami: A state-of-the-art review," *International Journal of Computer Assisted Radiology and Surgery* **12**(11), 2023–2032.

Kuribayashi, K. [2004] *A Novel Foldable Stent Graft* (Doctoral dissertation, Oxford University, UK).

Kuribayashi, K., Tsuchiya, K., You, Z., Tomus, D., Umemoto, M., Ito, T. and Sasaki, M. [2006] "Self-deployable origami stent grafts as a biomedical application of Ni-rich TiNi shape memory alloy foil," *Materials Science and Engineering: A* **419**(1–2), 131–137.

Lang, R. J., Tolman, K. A., Crampton, E. B., Magleby, S. P. and Howell, L. L. [2018] "A review of thickness-accommodation techniques in origami-inspired engineering," *Applied Mechanics Reviews* **70**(1).

Lee, D. Y., Kim, S. R., Kim, J. S., Park, J. J. and Cho, K. J. [2017] "Origami wheel transformer: A variable-diameter wheel drive robot using an origami structure," *Soft Robotics* **4**(2), 163–180.

Leon, S. E., Lages, E. N., De Araújo, C. N. and Paulino, G. H. [2014] "On the effect of constraint parameters on the generalized displacement control method," *Mechanics Research Communications* **56**, 123–129.

Liu, K. and Paulino, G. H. [2016] "MERLIN: A MATLAB implementation to capture highly nonlinear behavior of non-rigid origami," *Proceedings of IASS Annual Symposia,* Vol. 2016, No. 13. International Association for Shell and Spatial Structures (IASS), pp. 1–10.

Liu, K. and Paulino, G. H. [2017] "Nonlinear mechanics of non-rigid origami: an efficient computational approach," *Proceedings of the Royal Society A: Mathematical, Physical and Engineering Sciences* **473**(2206), 20170348.

Liu, R., Mcginty, S., Cui, F., Luo, X. and Liu, Z. [2019] "Modelling and simulation of the expansion of a shape memory polymer stent," *Engineering Computations* **36**(8), 2726–2746.

Liu, R., Xu, S., Luo, X. and Liu, Z. [2020] "Theoretical and numerical analysis of mechanical behaviors of a metamaterial-based shape memory polymer stent," *Polymers* **12**(8), 1784.

Liu, S., Lv, W., Chen, Y. and Lu, G. [2014] "Deployable prismatic structures with origami patterns," in *ASME 2014 International Design Engineering Technical Conferences and Computers and Information in Engineering Conference*, American Society of Mechanical Engineers Digital Collection.

Morgan, J., Magleby, S. P. and Howell, L. L. [2016] "An approach to designing origami-adapted aerospace mechanisms," *Journal of Mechanical Design* **138**(5), 052301.

Ogden, R. W. [1997] *Non-linear Elastic Deformations* (Dover Publications Inc.).

Onal, C. D., Wood, R. J. and Rus, D. [2012] "An origami-inspired approach to worm robots," *IEEE/ASME Transactions on Mechatronics* **18**(2), 430–438.

Peraza-Hernandez, E. A., Hartl, D. J. and Lagoudas, D. C. [2016] "Kinematics of origami structures with smooth folds," *Journal of Mechanisms and Robotics* **8**(6), 061019.

Peraza-Hernandez, E. A., Hartl, D. J., Malak Jr, R. J. and Lagoudas, D. C. [2014] "Origami-inspired active structures: a synthesis and review," *Smart Materials and Structures* **23**(9), 094001.

Rodrigues, G. V., Fonseca, L. M., Savi, M. A. and Paiva, A. [2017] "Nonlinear dynamics of an adaptive origami-stent system," *International Journal of Mechanical Sciences* **133**, 303–318.

Salerno, M., Zhang, K., Menciassi, A. and Dai, J. S. [2016] "A novel 4-DOF origami grasper with an SMA-actuation system for minimally invasive surgery," *IEEE Transactions on Robotics* **32**(3), 484–498.

Schenk, M. and Guest, S. D. [2011] "Origami folding: A structural engineering approach," *Origami* **5**, 291–304.

Schenk, M., Kerr, S. G., Smyth, A. M. and Guest, S. D. [2013] "Inflatable cylinders for deployable space structures," in *First Conference Transformables*, Seville, Spain, pp. 18–20.

Tachi, T. [2010] "Geometric considerations for the design of rigid origami structures," in *Proceedings of the International Association for Shell and Spatial Structures (IASS) Symposium,* (Elsevier Ltd), pp. 458–460.

Turner, N., Goodwine, B. and Sen, M. [2016] "A review of origami applications in mechanical engineering," *Proceedings of the Institution of Mechanical Engineers, Part C: Journal of Mechanical Engineering Science*, **230**(14), 2345–2362.

Vander Hoff, E., Jeong, D. and Lee, K. [2014] "OrigamiBot-I: A thread-actuated origami robot for manipulation and locomotion," in *2014 IEEE/RSJ International Conference on Intelligent Robots and Systems* (IEEE), pp. 1421–1426.

Zhou, C. H., Wang, B., Luo, H. Z., Chen, Y. W., Zeng, Q. H. and Zhu, S. Y. [2017] "Quasi-static axial compression of origami crash boxes," *International Journal of Applied Mechanics*, **9**(5), 1750066.